Mitsugumin 56 (hedgehog acyltransferase-like) is a sarcoplasmic reticulum-resident protein essential for postnatal muscle maturation

2016

范　博

CONTENTS

ABSTRACT

Mitsugumin 56 (MG56), also known as the membrane-bound O-acyl-transferase family member hedgehog acyltransferase-like, was identified as a new sarcoplasmic reticulum component in striated muscle. *Mg56*-knockout mice grew normally for a week after birth, but shortly thereafter exhibited a suckling defect and died under starvation conditions. In the knockout skeletal muscle, regular contractile features were largely preserved, but sarcoplasmic reticulum elements swelled and further developed enormous vacuoles. In parallel, the unfolded protein response was severely activated in the knockout muscle, and presumably disrupted muscle development leading to the suckling failure. Therefore, MG56 seems essential for postnatal skeletal muscle maturation.

INTRODUCTION

The sarcoplasmic reticulum (SR) is the powerful Ca^{2+}-handling organelle of muscle cells, and evolutionarily represents a highly specialized form of the endoplasmic reticulum (ER). During contractions of striated muscle, the activation of dihydropyridine receptors/L-type Ca^{2+} channels (DHPRs) in the transverse (T-) tubule opens ryanodine receptor channels (RyRs) to trigger SR Ca^{2+} release [1]. Such functional coupling between the T-tubular and SR Ca^{2+} channels takes place in junctional membrane complexes formed by junctophilins (JPs), *i.e*. the triad in skeletal muscle and the diad in cardiac muscle [2-5]. The SR region closely associated with the T-tubule is called the junctional SR or the terminal cisternae, and contains abundant JPs and RyRs to control Ca^{2+} release. The rest of the SR portion, called the longitudinal SR, is responsible for Ca^{2+} uptake mediated by enriched SR/ER Ca^{2+}-ATPase (SERCA). The major SR Ca^{2+}-handling proteins, including RyRs, SERCA, and luminal Ca^{2+}-binding proteins, have been extensively characterized, and such studies have deepened our

understanding of intracellular Ca^{2+} stores. However, there are still many SR components with no functional annotation, and it is also important to examine such as-yet-unknown proteins in striated muscle. In this paper, I report the identification of a new SR protein, designated mitugumin 56 (MG56)/hedgehog acyltransferase-like protein (HHATL), and describe its essential role in the integrity of the skeletal muscle SR.

ABBREVIATIONS

EDL, extensor digitorum longus;

ER, endoplasmic reticulum;

ERAD, endoplasmic reticulum-associated degradation;

DHPR, dihydropyridine receptor;

HHATL, hedgehog acyltransferase-like;

IP_3R, inositol trisphosphate receptor;

JP, junctophilin;

LC-MS/MS, liquid chromatography-tandem mass spectrometry;

MBOAT, membrane-bound O-acyltransferase;

MG56, mitsugumin 56;

P, postnatal day;

RyR, ryanodine receptor;

SERCA, SR/ER Ca^{2+}-ATPase;

SR, sarcoplasmic reticulum;

TA, tibialis anterior;

T-tubule, transverse tubule;

UPR, unfolded protein response.

RESULTS

Identification of muscle-specific MG56/HHATL

During the course of our screening [6-8], MG56 was identified as a new SR protein from rabbit skeletal muscle. Purified rabbit MG56 was analyzed with an automated Edman sequencer to yield the N-terminal sequence of 17 residues (GVKTALPAAELGLYSLV in one-letter code). The determined sequence is almost identical to those of the hypothetical HHATL proteins deduced from mouse and human databases (16/17 identity). Therefore, MG56 corresponds to the rabbit HHATL counterpart. Paying attention to the primary structure (Fig. 1A), MG56/HHATL contains an MBOAT (membrane-bound O-acyltransferase) motif and multiple transmembrane segments. Among the MBOAT family members, MG56 has high sequence similarity with vertebrate HHAT, and these proteins form a sub-cluster together with the invertebrate HHAT-related proteins and yeast Gup proteins, all of which bear no functional annotations in databases (Fig. 1B).

MBOAT family proteins so far characterized are enzymes localized to the ER (Fig. 1C). For example, lysophospholipid acyltransferases (MBOAT1, MBOAT2, MBOAT7 and LPCAT3) and acyl-CoA:cholesterol acyltransferases (ACAT1 and ACAT2) transfer fatty acids onto hydroxyl groups of membrane-bound lipids [18]. As additional examples in this family, HHAT, ghrelin O-acyltransferase (GOAT) and Porcupine (PORCN) contribute to unique post-translational modification in the ER by transferring fatty acids to the specific secretory peptides [16,19,20]. Therefore, in the same manner as other MBOAT family members, MG56 might mediate fatty acylation in the intracellular membrane (Fig. 1D). However, the MG56 gene function is unknown, although it has been reported that MG56/HHATL does not catalyze the fatty acylation of sonic hedgehog [21].

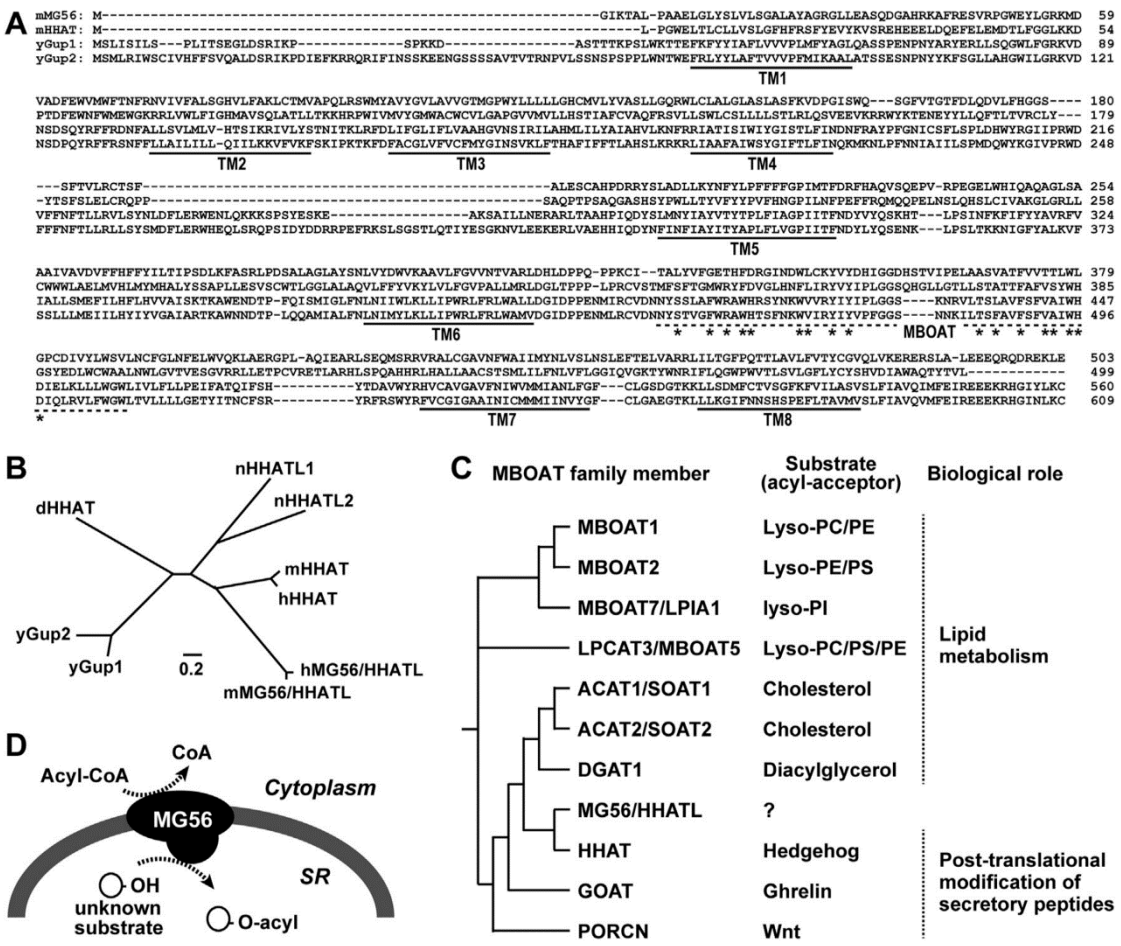

Figure 1. Identification of MG56/HHATL in muscle.

(A) Sequence alignment of mouse MG56, mouse HHAT, yeast Gup1 and yeast Gup2. The MBOAT motif and putative transmembrane segments (TM1-8) were tentatively assigned according to a previous report [16]. In the 17 aligned positions marked by asterisks, residues are well-conserved among the family members [18], and contribute in part to acyltransferase activity in the case of porcupine [35]. Deletions are indicated by gaps (-), and residue numbers are given on the right-hand sides of individual lines. (B) Phylogenic tree of MG56-related proteins. Homology searches of MG56 in public databases yielded MG56-related proteins encoded in the yeast (y), invertebrate (fruit fly, d; nematode, n) and mammalian (mouse, m; human, h) genomes. Sequence data were analyzed using the Clustal W software (DDBJ, http://www.ddbj.nig.ac.jp/index-j.html), and the scale bar indicates substitution per aligned site. (C) Mammalian MBOAT family members. The primary structures of the mouse family members were analyzed using the Clustal W algorithm to yield the phylogenetic tree. Lipid and peptide substrates are listed in the catalytic reactions mediated by the family members. (D) Schematic representation of the proposed MG56 catalytic activity in muscle SR.

Junctional SR-resident MG56 in skeletal muscle

My Northern blot analysis in mouse tissues indicated that MG56 is predominantly expressed in skeletal and cardiac muscle. The proposed muscle-specific expression was further confirmed by Western blot analysis (Fig. 2A). However, MG56 with a calculated molecular mass of 56 kDa was detected as 40~45-kDa protein bands, despite the fact that the specific reactivity of our antibody was biochemically and histochemically demonstrated by the loss of the immunosignals in knockout mice (see below). The reason for the multiple MG56 bands was unknown: its highly-hydrophobic structure might underlie a couple of denatured conformations; alternatively, post-translational modifications, such as glycosylation or phosphorylation, could result in different molecular sizes.

In longitudinal sections of mature skeletal muscle, MG56-immunoreactivity formed a clear striation-staining pattern at the A-I junction, suggesting its specific localization in the triad junction (Fig. 2B). By means of sucrose density gradient centrifugation, muscle microsomes can be separated into several fractions; the T-tubule, longitudinal SR and junctional SR are enriched in low, intermediate, and high-density fractions, respectively [22]. In this separation process, MG56 was highly enriched in the junctional SR fraction (Fig. 2C). Moreover, the MG56 and RyR/JP signals were approximately merged in the immunohistochemical staining and co-enriched in the membrane preparation. Therefore, MG56 is specifically localized in the junctional SR in mature skeletal muscle.

As is the case for other SR Ca^{2+}-handling proteins, MG56 expression is highly induced during postnatal development (Fig. 2D), suggesting the possibility that MG56 might exert a muscle-specific role together with certain binding partners in the triad junction. To survey protein-protein

interactions, I treated SR membrane preparations with chemical crosslinkers and examined the migration shift of MG56. However, Western blotting detected no difference in mobility before and after crosslinking, indicating that MG56 exists primarily in a monomeric form in the junctional SR.

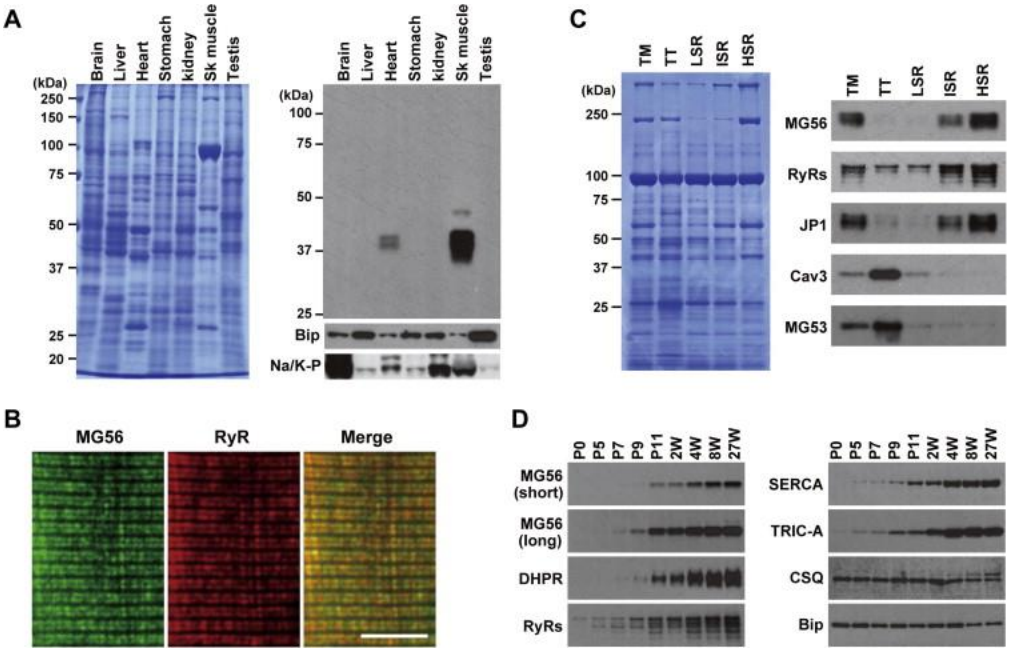

Figure 2. Biochemical characterization of MG56.

(A) Western blot analysis of mouse tissue microsomes using antibody specific to MG56. Total microsomal proteins from mouse tissues (5 μg protein/lane) were separated by SDS-PAGE and subjected to Coomassie staining (left panel), or to immunoblot analysis using antibody specific to MG56 (right panel). Bip and Na-K pump (Na/K-P) were also detected as loading markers. (B) Immunohistochemical detection of MG56 in mouse skeletal muscle. A longitudinal section was stained with antibodies to MG56 and RyR, and subjected to confocal microscopic observation. Scale bar, 10 μm. (C) Distribution of MG56 in muscle membrane preparations. Total microsomal (TM), T-tubular (TT), light SR (LSR), intermediate SR (ISR), and heavy SR (HSR) fractions were prepared from mouse skeletal muscle. The membrane preparations (5 μg/lane) were analyzed by SDS-PAGE and Coomassie staining (left panel), and also subjected to immunoblot analysis using antibodies specific to MG56 and maker proteins (right panel). RyRs (RyR1 and RyR3) and JP1 are heavy SR markers, while caveolin-3 (Cav3) and MG53 are T-tubular markers. (D) Postnatal MG56 expression. Total muscle microsomes were prepared from mice at various developmental stages, from neonates (P0) to 27-week-old mice (27W). Microsomal proteins were analyzed by Western blotting using antibodies specific to MG56, RyRs, DHPR, JP1, triadin, SERCA1, TRIC-A and Bip/GRP78.

Postnatal lethality in Mg56-knockout mice

I constructed a replacement vector to introduce a targeted deletion in the 5′-terminal region of the *Mg56* gene and generated knockout mice on the C57BL/6 genetic background (Fig. 3A-C). The resulting heterozygous mutant mice were healthy, exhibiting normal development and reproduction. Cross-breeding between the heterozygous mutants produced *Mg56*-knockout neonates with a Mendelian ratio. *Mg56*-knockout mice showed regular locomotion and grew normally during the postnatal lactation period, but stopped growing approximately on postnatal day 7 (P7) and gradually lost body weight thereafter (Fig. 3D). All of the knockout mice were severely debilitated and died within two weeks after birth (Fig. 3E), even though mother mice engaged in pup-rearing irrespective of the genotypes.

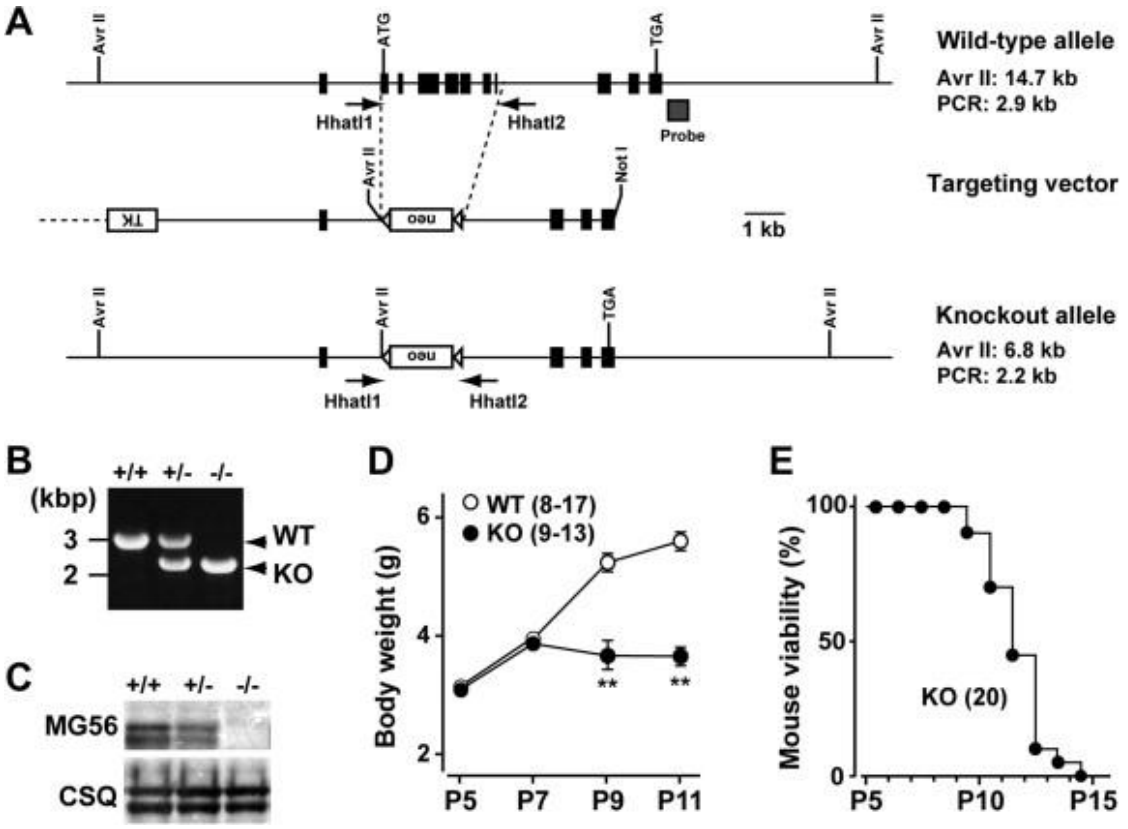

Figure 3. Generation of *Mg56*-knockout mice.

(A) Homologous recombination at the *Mg56* locus. The restriction maps of the wild-type allele, targeting vector, and mutant allele are illustrated. The exons, the neomycin resistance gene (neo), and the thymidine kinase gene (TK) are indicated by boxes. For Southern blot detection of the homologous recombination, genomic DNAs from embryonic stem cells were digested with the restriction enzyme *Avr* II and examined using the hybridization probe indicated. For PCR genotyping, genomic DNA preparations were amplified using the primer set indicated by arrows. (B) Detection of mutant gene in PCR. Genomic DNA preparations were used as templates, and the amplified DNA fragments were analyzed on an agarose gel; the products derived from the wild-type and mutant allele are indicated. (C) Western blot analysis of MG56 in skeletal muscle. Total microsomal proteins from mouse hindlimbs were separated by SDS-PAGE and analyzed with antibodies against MG56 and calsequestrin subtypes (CSQ1 and CSQ2). (D) Postnatal body weight change in *Mg56*-knockout mice. The data represent the mean ± S.E.M. Statistical differences between the genotypes are marked with asterisks ($^{**}P < 0.01$ in *t*-test). (E) Postnatal survival rate in *Mg56*-knockout mice. The numbers of mice examined are shown in parentheses.

The weight reduction was most likely due to suckling failure in *Mg56*-knockout mice, because their gastric milk contents were clearly insufficient after P7 (Fig. 4A). Accordingly, blood glucose and plasma triglyceride levels were severely reduced on P9 and P11, while circulating ketone bodies and free fatty acids were remarkably elevated as the knockout mice neared death (Fig. 4B). Therefore, *Mg56* deficiency results in a slow death by starvation during the lactation period. There were no cases of sudden death, cyanosis, gastro-esophageal reflux or behavioral episode indicative of paralysis/epilepsy detected in the knockout mice, suggesting that cardiac, diaphragmatic and/or neural defects were not associated with the lethality. Based on these observations, together with the gene expression profile, *Mg56* deficiency may result in skeletal muscle dysfunction leading to suckling failure.

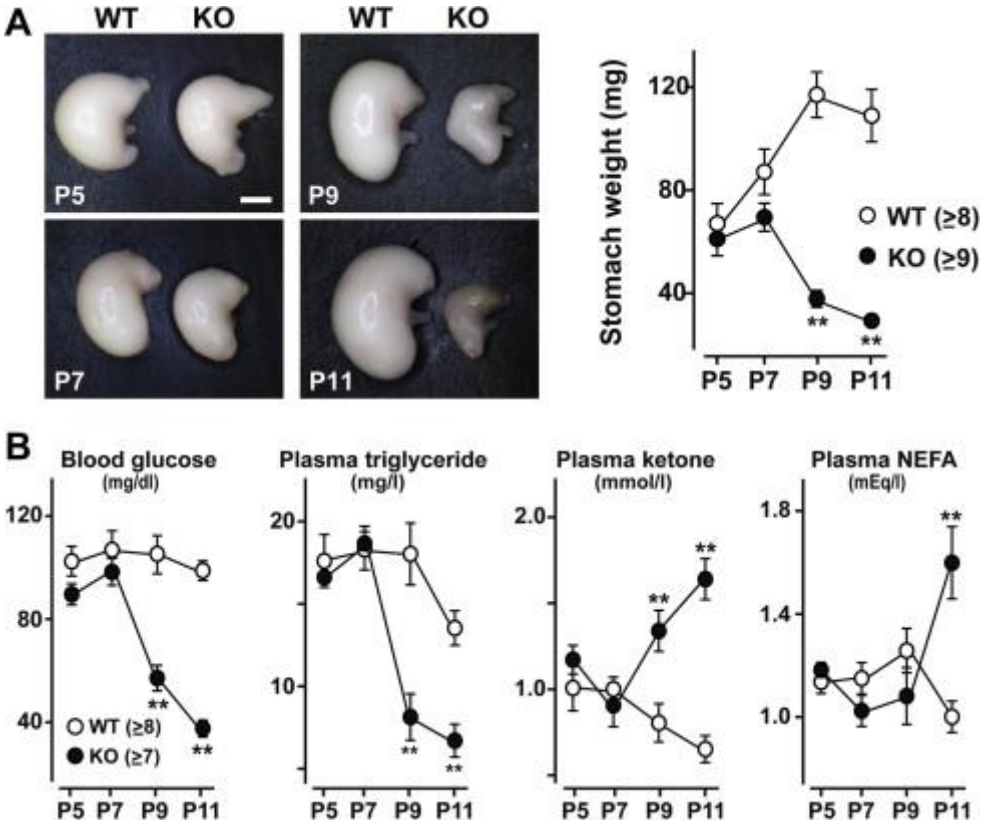

Figure 4. Suckling defect and malnutrition in *Mg56*-knockout mice.

(A) Insufficient stomach milk contents in *Mg56*-knockout mice. Representative stomach images were taken from the P5-11 knockout mice, and the dissected stomachs were weight-checked. The stomachs from infant mice exhibit milky color, but insufficient milk contents were observed in the knockout mice after P7. Scale bar, 2 mm. (B) Starvation state detected by blood tests in *Mg56*-knockout mice. The blood samples collected were directly used for glucose measurement. After blood cell separation, the recovered plasma samples were biochemically tested for triglyceride, ketone body and non-esterified fatty acids (NEFA). The data represent the mean ± S.E.M., and the numbers of mice examined are shown in parentheses. Statistical differences between the genotypes are indicated with asterisks ($^{**}P < 0.01$ in *t*-test).

Vacuole formation in Mg56-knockout muscle

I morphologically analyzed skeletal muscle in *Mg56*-knockout mice. In thigh muscle from P5 *Mg56*-knockout mice, the sectioned profiles of SR elements appeared to be dilated in considerable portions (Fig. 5A). The percentage of muscle fibers containing such swollen elements was moderate (11.6 ± 5.4%, n = 4 mice) in P5 knockout mice, but the SR dilation broadened and became more prominent so as to generate spherically extended vacuoles in P7 knockout mice (45.6 ± 12.4%, n = 3 mice). Small SR vacuoles were predominantly detected near the Z-line (Fig. 5A-C), indicating that SR swelling starts in the I-band region. These swollen elements most likely expand and further distort the normal SR architecture, since enlarged vacuoles extensively developed, whereas regular SR elements disappeared in most of the P9 knockout fibers. Furthermore, the enlarged vacuoles appeared to fuse together to generate enormous vacuoles, radiating outward from the Z-line region, encompassing the sarcomere and surrounding myofibrils (Fig. 5F-H). Therefore, *Mg56* deficiency results in SR swelling and further disrupts the SR network in skeletal muscle (Fig. 5I). Fast and slow-twitch muscle fibers can be roughly assigned by reference to the Z-line thickness [23], but regardless of the fiber type, SR dilation was evenly distributed. Although triad formation was actively ongoing at the early lactational stages, no morphological abnormalities were detected in the triad junction or T-tubule in the knockout muscle, indicating that MG56 has no architectural role in muscle-specific junctional membrane structures.

Within the swollen SR observed in the P5 and P7 knockout mice, electro-dense deposits were frequently detected (Fig. 5D), and were revealed to be “myelin figures” (lipid-rich multi-lamellar structures) in high magnification images (Fig. 5E). Such lipid-rich deposits were not detected in the control

SR of wild-type muscle. In the enlarged vacuoles of the P9 knockout muscle, I occasionally detected linear lipid aggregates that may be excessive membranes collaterally generated by fusion between vacuolated SR elements (Fig. 5F). Interestingly, electron-dense materials including myelin figures and soluble proteins were essentially absent from the enlarged vacuoles in the knockout muscle. Within these empty SR vacuoles, intraluminal substances may have been randomly degraded leading to osmotic imbalance and organelle dysfunction.

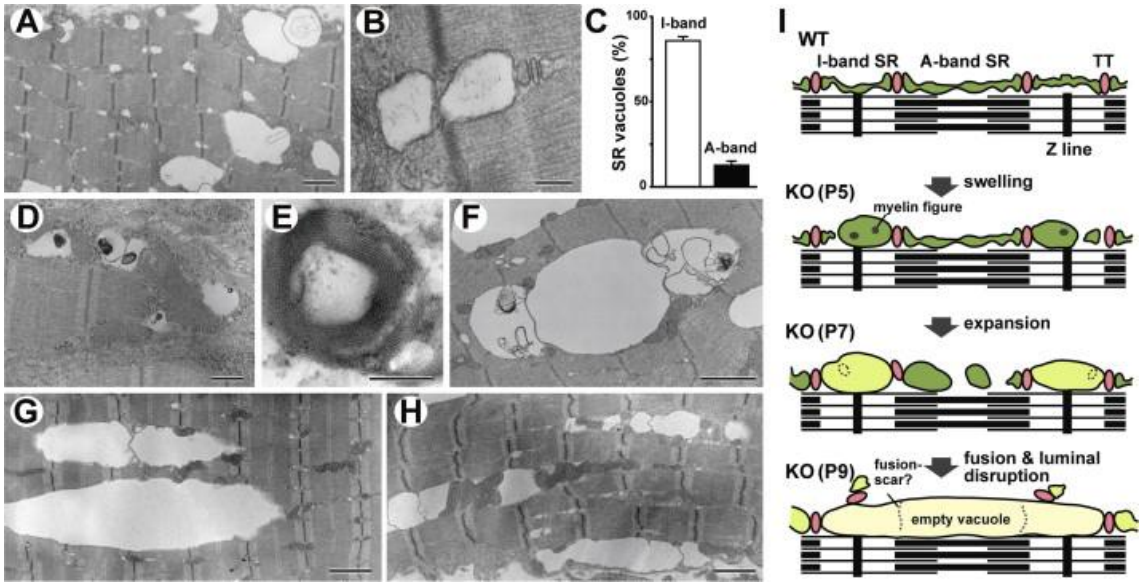

Figure 5. SR dilation and vacuole formation in *Mg56*-knockout muscle.

The T-tubule and triad junction were normally formed in *Mg56*-knockout muscle, however, SR swelling was frequently detected on P5 (A) and became more frequent afterwards. The SR dilation seemed to start at the I-band SR, because small vacuoles were predominantly detected in the vicinity of the Z-line (B). In the statistical analysis of the P7 knockout mice (n = 3), small vacuoles (0.1-0.3 μm in diameter, >244 vacuoles in each mouse) were predominantly detected to the I-band site (C). The data represent the mean ± S.E.M. Electron-dense deposits were occasionally observed in dilated SR elements in the P5 and P7 knockout mice (D) and assigned as myelin figures on high-magnification observation (E). Dilated SR elements probably fused together to further develop into enlarged vacuoles (F). Enormous vacuoles encompassing sarcomere units were frequently observed in the P9 knockout muscle regardless of the fiber type; fast (G) and slow (H) muscle fibers were tentatively assigned based on the Z-line thickness. Scale bars, 1 μm in A, F, G and H; 500 nm in D; 200 nm in B; 100 nm in E. (I) Proposed scheme for vacuole generation and development in *Mg56*-knockout muscle.

Disrupted development of contractility in Mg56-knockout muscle

Light microscopy also detected the formation of the SR vacuoles in *Mg56*-knockout muscle fibers (Fig. 6A). In extensor digitorum longus (EDL) bundles from the knockout mice, ~25% of the muscle fibers contained the SR vacuoles on P7, and further enlarged vacuoles were observed in >70% of fibers on P9. No differences in the vacuolar characteristics were detected before and after fatigue-induced electrical stimuli in the knockout muscle, suggesting that vacuolar development is not dependent on SR Ca^{2+} cycling (Fig. 6B). Meanwhile, the triad junction contains a set of signaling proteins to convert depolarization into the intracellular Ca^{2+} signal for muscle contraction. Western blot analysis demonstrated that the major components for excitation-contraction coupling, including RyR, DHPR, SERCA and JP, were normally expressed in *Mg56*-knockout muscle.

A major SR function is Ca^{2+} handling, and the loss of Ca^{2+}-handling proteins often leads to SR swelling in striated muscle [9,11,24]. Thus, I next focused on the contractility of *Mg56*-knockout EDL muscle to survey any irregular SR Ca^{2+} handling (Fig. 6C-E). Assuming that *Mg56* deficiency might affect SR Ca^{2+} handling, impaired Ca^{2+} release and/or storage would primarily affect the force-frequency relationship, while decelerated Ca^{2+} uptake would directly expand the relaxation phase after contraction. Of course, these functional abnormalities are not independent and would be expected to interact synergistically; for example, prolonged relaxation above a threshold level facilitates force summation during tetanic stimuli so as to indirectly affect the force-frequency relationship. In EDL bundles from P7 *Mg56*-knockout mice, apparently normal contractile responses were evoked by electrical stimuli, while the half relaxation time of twitch contraction was slightly extended, suggesting weakened Ca^{2+} uptake. However, the proposed

impairment of Ca^{2+} uptake seems functionally minimal, because the knockout muscle retained a normal force-frequency relationship. These observations indicate that *Mg56* deficiency does not severely damage SR Ca^{2+}-handling in P7 muscle. However, in the P9 knockout muscle, in addition to prolonged relaxation, severe impairment of force generation was observed; the force-frequency relation was shifted downward without any accompanying altered qualitative characteristics compared with control. From a different viewpoint, muscle contractility during P7-9 was remarkably enhanced in wild-type mice, but marginally reduced in the knockout mice. Therefore, in the P9 knockout EDL bundles, the weakened tension seems to reflect disrupted development as well as dysfunctioning SR Ca^{2+} handling in the vacuole-containing fibers.

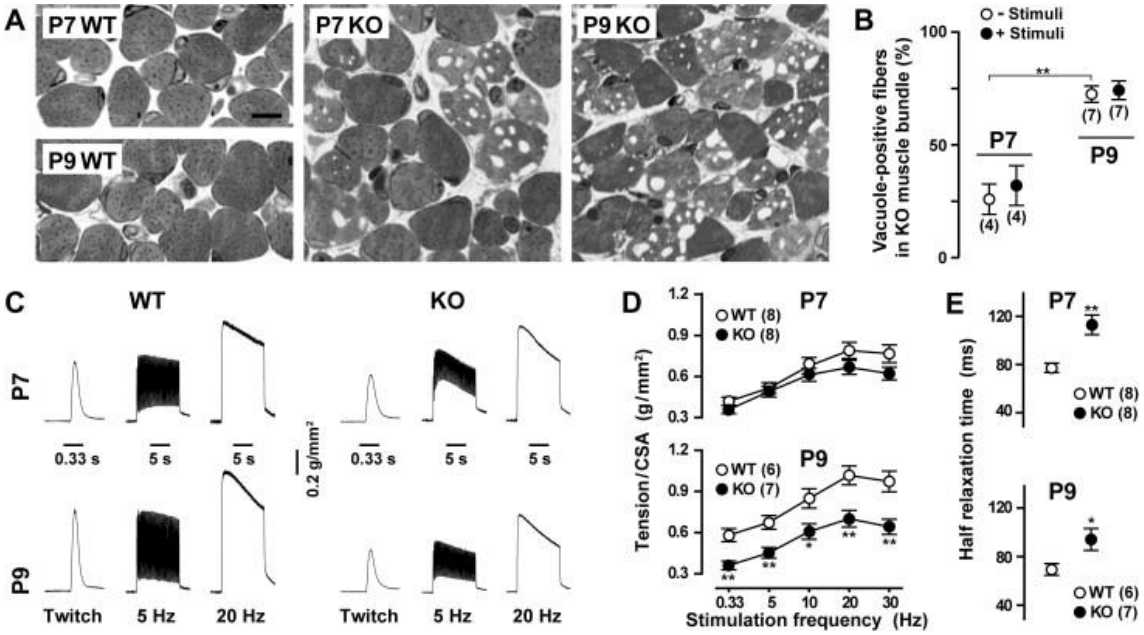

Figure 6. Diminished contractile ability in *Mg56*-knockout muscle.

(A) Histological detection of vacuole-positive*Mg56*-knockout EDL muscle fibers. EDL bundles were fixed and stained with toluidine blue for microscopic observation. Scale bar, 10 μm. (B) Population of vacuole-containing fibers in *Mg56*-knockout EDL bundles. EDL bundles were treated with or without fatigue-induced electrical stimuli (15 Hz for 10 min × 2) for the analysis. The data represent the mean ± S.E.M., and the numbers of mice examined are shown in parentheses. The rate of vacuole-positive fibers is significantly different between the P7 and P9 bundles ($^{**}P < 0.01$), although the increased tendency of vacuole-positive fibers upon fatigue-induced stimuli is not significant. (C) Isometric tension monitoring in *Mg56*-knockout EDL muscle. Representative recording data from P7 and P9 mice are shown. (D) Force-frequency relationship in *Mg56*-knockout and wild-type EDL muscle. The developed contractile responses were normalized to cross sectional area (CSA) in each muscle bundle. The P7 knockout muscle retained an apparently normal force-frequency relationship. In the P9 knockout muscle, contractile responses were reduced overall, and the force-frequency curve was shifted downward. (E) Prolonged relaxation phase in *Mg56*-knockout EDL muscle. The half-relaxation time was analyzed in the twitch responses. The data represent the mean ± S.E.M., and the numbers of muscle bundles examined are shown in parentheses. Statistical differences between the genotypes are indicated with asterisks ($^{*}P < 0.05$, $^{**}P < 0.01$ in *t*-test). It was very difficult to prepare the intact specimens, because EDL muscle was immature and fragile in the suckling mice. Accordingly, some EDL bundles exhibited blunt and weak responses in contraction recording, likely due to artificial handling damages. For each experimental group, the specimens developing weak twitch responses that ranked in the bottom ~30% (P7 WT, 4/12; P9 WT, 2/9; P7 KO, 4/12; P9 KO, 3/10) were eliminated for the statistical analysis.

Compared with the contractile and morphological abnormalities, SR swelling clearly precedes the contractile impairment in *Mg56*-knockout skeletal muscle. The set of muscles controlling milk suckling might also start to reduce their contractile efficiency around P7-9, because anatomical observations indicated that all of the working muscles develop SR vacuoles in the knockout mice. Meanwhile, I also focused on the hearts in the P9 knockout mice. In contrast to the drastic defects in the knockout skeletal muscle, both morphological and functional features were largely maintained in the knockout heart, as assessed by microscope, echocardiography and electrocardiography (Fig. 7). Therefore, it is unlikely that cardiac defects directly contribute to the suckling defect and lethal phenotype in the knockout mice.

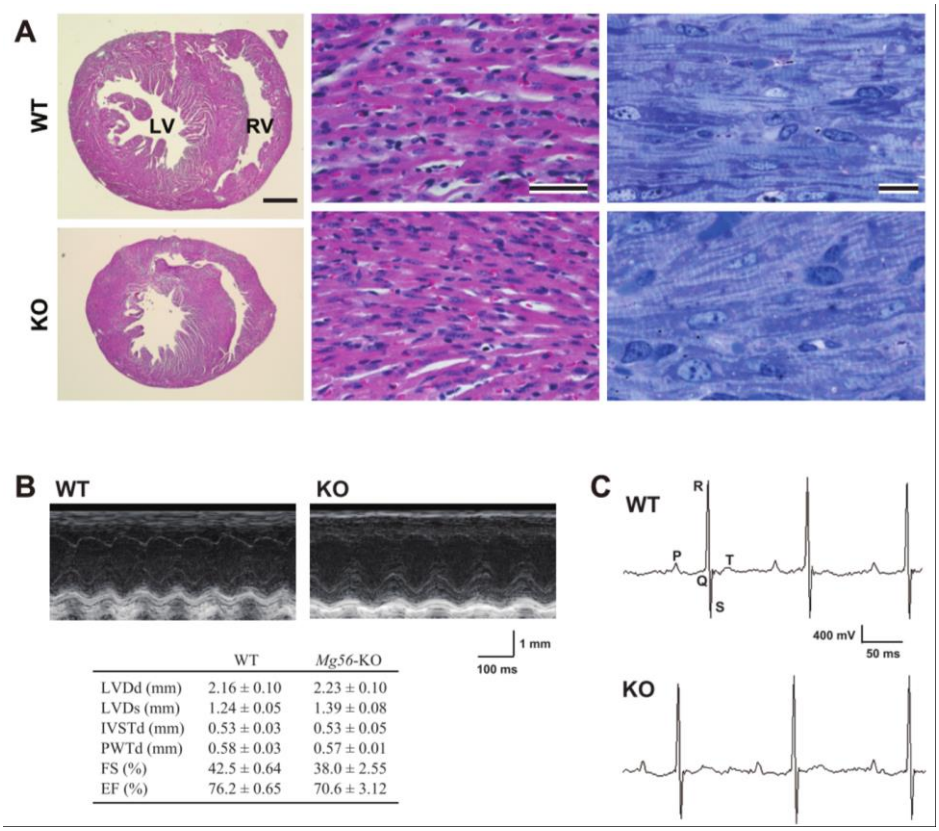

	WT	*Mg56*-KO
LVDd (mm)	2.16 ± 0.10	2.23 ± 0.10
LVDs (mm)	1.24 ± 0.05	1.39 ± 0.08
IVSTd (mm)	0.53 ± 0.03	0.53 ± 0.05
PWTd (mm)	0.58 ± 0.03	0.57 ± 0.01
FS (%)	42.5 ± 0.64	38.0 ± 2.55
EF (%)	76.2 ± 0.65	70.6 ± 3.12

Figure 7. Apparently normal features in P9 *Mg56*-knockout hearts.

(A) Representative images of cardiac sections. Cross-sections of ventricles (left panels, scale bar, 0.5 mm). LV, left ventricle. RV, right ventricle. Histological sections of HE-stained ventricular regions (middle panels, scale bar, 50 μm). High magnification images of toluidine blue-stained ventricular muscle (right panels, scale bar 10 μm). The P9 Mg56-knockout hearts were slightly smaller than controls, because the knockout mice stopped growing on ~P7. However, the knockout hearts exhibited no histological abnormalities, and SR swelling was not detected in the knockout cardiomyotes. (B) Representative echocardiographic images. P9 wild-type (n=5) and Mg56-knockout (n=3) mice were subjected to M-mode assessment, and parameters monitored were statistically analyzed (inset table). Left ventricular chamber dimensions measured are internal dimension diastole (LVDd), internal dimension systole (LVDs), interventricular septum thickness diastole (IVSTd), and posterior wall thickness diastole (PWTd). Based on the measurements, left ventricular fractional shortening (FS) and ejection fraction (EF) were calculated. The data represent mean ± SEM. No significant differences were observed between the genotypes, indicating no heart failure-related diagnostic in the knockout mice. (C) Representative electrocardiogram recording charts. Similar PQRST waves were detected in P9 wild-type and Mg56-knockout mice (n>4 in each group). Heart rate tended to be slightly slower in Mg56-knockout mice likely due to the malnutrition conditions. However, no arrhythmia-related changes, such as T inversion, wide QRS complex and QT prolongation, were detected in the knockout mice.

ER stress in Mg56-knockout muscle

To roughly survey altered gene expression in *Mg56*-knockout muscle, total RNA preparations from lower limb muscle were subjected to gene microarray analysis. Data comparison between the genotypes indicated that an extensive set of transcripts with the "ER stress" annotation was upregulated in the knockout muscle (Fig. 8).

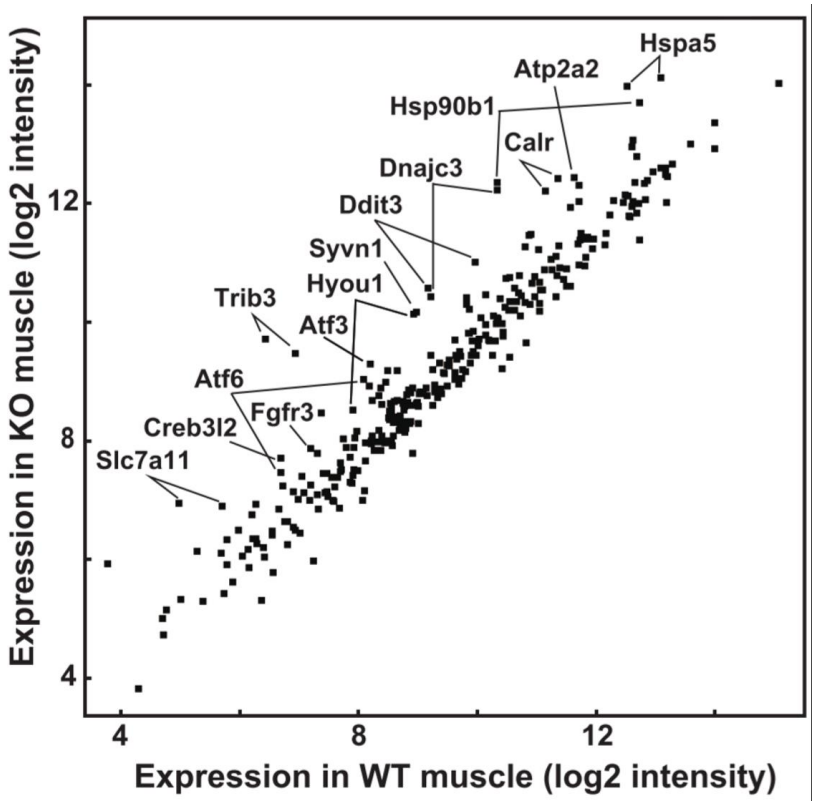

Fig. 8. Gene expression comparison between *Hhatl*-knockout and wild-type muscle. Total TA muscle RNA preparations from three P9 mice were mixed in equal amounts and subjected to microarray analysis in order to exhaustively evaluate the mRNA content. The data for genes annotated as "apoptosis" and "ER stress" were selected to draw the scatter plot. Hspa5, 78-kda glucose-regulated protein GRP 78; Hspb1, GRP 94; Calr, calreticulin; Atp2a2, SR/ER Ca2+-ATPase 2; Dnajc3, P58(IPK); Syvn1, E3 ubiquitin ligase synoviolin; Ddit3, C/EBP homologous protein (CHOP); Hyou1, GRP 170; Atf3, cAMP-dependent transcription factor ATF-3; Atf6, ATF-6; Trib3, pseudokinase tribbles homologue 3; Fgfr3, fibroblast growth factor receptor 3; Creb3l2, cAMP-responsive element binding protein 3 like 2; Slc7a11, solute carrier family 7 member 11 (y+ system transporter).

Based on this observation, together with the fact that unfolded protein response (UPR) is often accompanied by ER dilation in various cell types [25-27], I next focused on ER stress in the knockout muscle. Various types of ER stress stimulate three major UPR pathways respectively mediated by ATF6 (activating transcription factor 6), IRE1α (inositol-requiring enzyme 1α), and PERK1 (protein kinase RNA-like ER protein kinase 1) [26]. The downstream effect of the UPR pathways is the induction of ER stress-related genes; for example, ATF6 activation induces *Grp94* (94-kDa glucose-regulated protein) and *Bip*/*Grp78* (78-kDa chaperone of the HSP70 family), while *Erdj4/Mdg1* (DnaJ family ER chaperone), and *Asns* (asparagine synthase) are induced under IRE1α and PERK1 activation, respectively. Quantitative RT-PCR analysis using RNA preparations from hind-limb tibialis anterior (TA) muscle clearly indicated that all of UPR pathways were highly activated in *Mg56*-knockout muscle during P7-P9 (Fig. 9). In contrast, the upregulation of ER stress-related gene expression was rather modest in the knockout diaphragm and essentially negligible in the knockout heart. Moreover, in wild-type mice under starvation conditions, TA muscle maintained normal expression of the UPR-related genes. Therefore, *Mg56* deficiency seems to preferentially activate ER stress-induced UPR in working muscle during the lactation period.

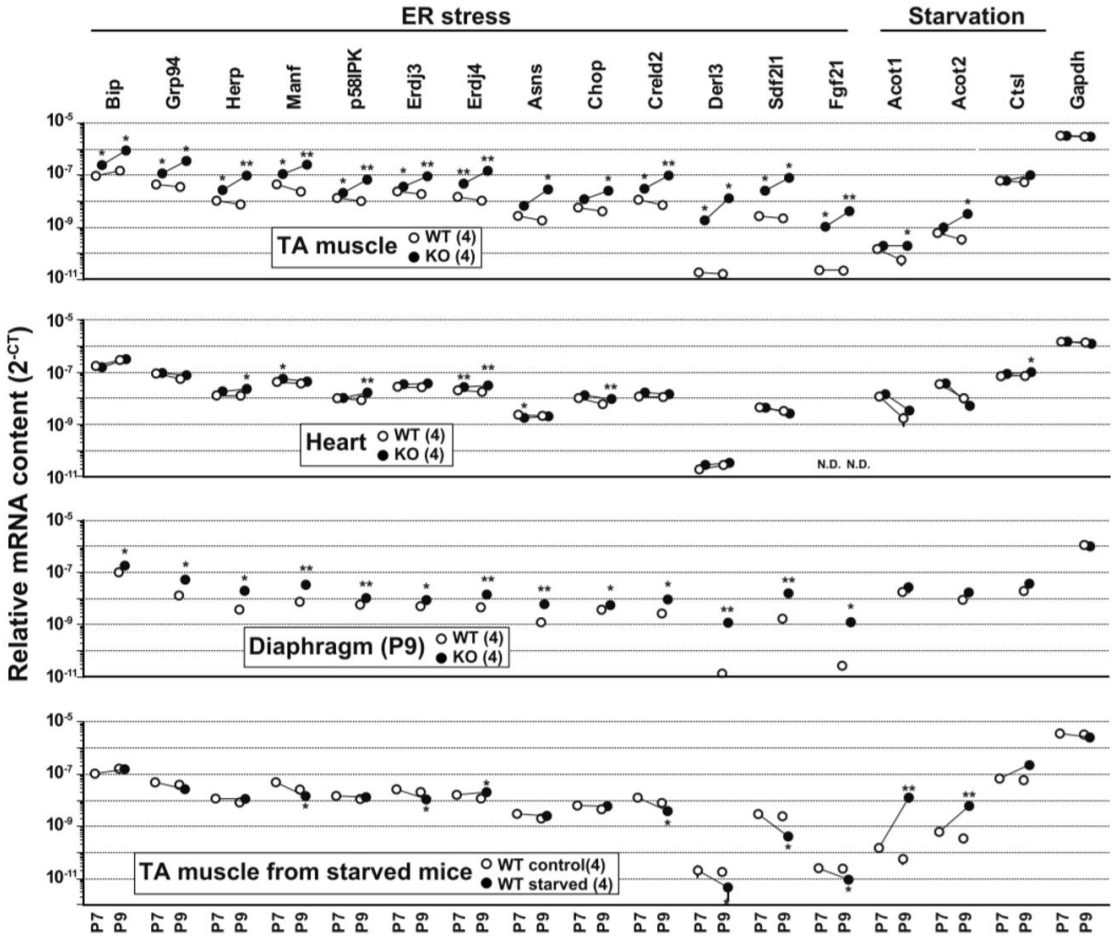

Figure 9. Upregulated expression of ER stress-related genes in *Hhatl*-knockout muscle.

Total RNAs were prepared from TA muscle, heart and diaphragm of P7 or P9 mice with or without starvation treatment for two days. To analyze the expression of representative ER stress and starvation-related genes, the RNA preparations were examined by quantitative RT-PCR using specific primer sets. The cycle threshold (Ct) indicates the cycle number at which the amount of amplified cDNA reaches a fixed threshold in each reaction. The data represent the mean ± SEM., and the numbers of mice examined are shown in parentheses. Statistical differences between groups are indicated by asterisks (*p<0.05, **p<0.01 in t-test).

IRE1α activation under ER stress enhances its intrinsic RNase activity, which converts the unspliced form of X box-binding protein 1 mRNA (XBP1u) into the spliced form (XBP1s) to produce an active transcription factor [28]. RT-PCR clearly detected significant XBP1s generation in *Mg56*-

knockout muscle (Fig. 10A). In cells undergoing ER stress, activated PERK phosphorylates the eukaryotic initiation factor eIF2α to inhibit cellular protein synthesis [25]. The knockout muscle abundantly contained the phosphorylated form of eIF2α, and also exhibited increased expression levels of GRP94 and Bip (Fig. 10B). These observations confirmed the activation of the three major UPR pathways in *Mg56*-knockout muscle. In addition, several proteins involved in the ER-associated degradation (ERAD) pathway, such as *Erdj4* and *Derl3*, are induced upon severe stress to resolve ER-luminal components in a non-specific manner [27]. RT-PCR clearly detected upregulated expression of *Erdj4* and *Derl3* in the knockout muscle (Fig. 9), suggesting that activated ERAD takes part in the generation of the empty SR vacuoles (Fig. 5F-H). The biochemical data, taken together, suggest that postnatal muscle maturation is disrupted under UPR and ERAD-activated conditions in *Mg56*-knockout mice.

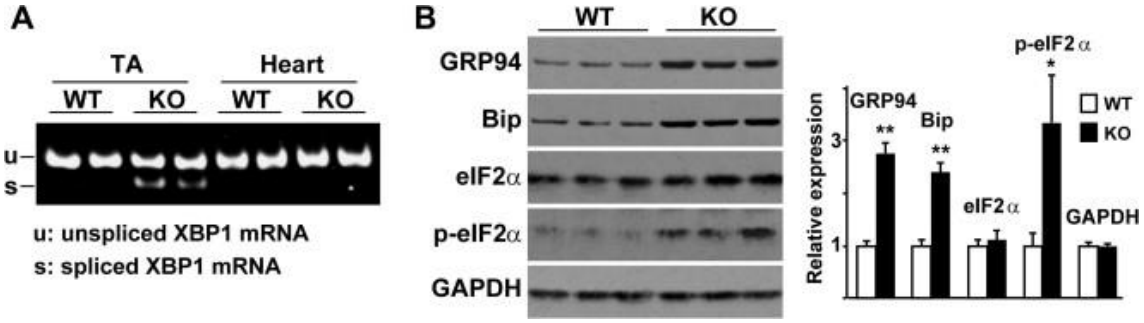

Figure 10. Biochemical detection of UPR activation in *Mg56*-knockout muscle.

(A) Induction of XBP1 mRNA splicing in *Mg56*-knockout muscle. Total RNA preparations from P9 muscle and heart muscle were subjected to RT-PCR to amplify DNA fragments derived from both the unspliced form (XBP1u, 234 bp) and the spliced form (XBP1s, 208 bp). The resulting fragments were analyzed by acrylamide gel electrophoresis. (B) Elevated UPR-related protein contents in *Mg56*-knockout muscle. Total lysates from P9 TA muscle were examined by Western blotting using antibodies against UPR marker proteins. GAPDH was analyzed as an internal control. p-eIF2α, phosphorylated form of eIF2α.

Discussion

During postnatal development in skeletal muscle, T-tubular extension and triad formation take place in parallel, and the longitudinal and junctional SR compartments also undergo extensive maturation processes [3]. In this thesis, I have identified MG56/HHATL as a new component of the junctional SR (Figs. 1 and 2) and determined its essential contribution to postnatal development during the suckling stages (Figs. 3 and 4). The evidence also shows that progressive SR swelling (Fig. 5) probably underlies UPR activation in *Mg56*-knockout muscle (Fig. 10). Although the knockout muscle exhibited a slow relaxation phase before developing severe contractile impairment (Fig. 6), it is unlikely that the junctional SR-resident MG56 directly modulates the Ca^{2+}-pumping activity of the longitudinal SR. The weak relaxation may have been caused by impaired SR Ca^{2+}-handling functions indirectly induced under ER stress conditions. Based on the data presented here, *Mg56* deficiency seems to stimulate ER stress-induced UPR, and thus disrupts postnatal development of working skeletal muscle leading to the progressive suckling failure and malnutrition. On the other hand, despite its specific residency in the junctional SR, MG56 has no evident role in triad formation or excitation-contraction coupling.

In *Mg56*-knockout muscle, I observed SR swelling as a common ultrastructural feature in ER stress-bearing cells, and also detected obvious UPR activation. It has been established that ER stress is induced by the perturbation of membrane lipid composition, as well as by the accumulation of unfolded proteins [25-30]. Meanwhile, the known MBOAT family members are enzymes mediating fatty-acylation, and therefore, MG56 may catalyze acylation in lipid or protein substrates (Fig. 1D). If lysophospholipid species were substrates in the presumed MG56-mediated reaction, a dramatic change

in SR lipid composition would be expected during postnatal muscle maturation. Additionally, the myelin figures detected in the swollen SR (Fig. 5 E) might be irregularly generated from the abnormal lipid composition. However, the LC-MS/MS analysis detected no significant changes in the major phospholipid contents between muscle microsomes from P9 *Mg56*-knockout and wild-type mice (Fig. 11). Therefore, at present I cannot predict lipid candidates for MG56 substrates. Conversely, assuming that MG56 can mediate acylation of an SR protein, knockout mice lacking MG56 and its substrate might develop similar pathophysiological phenotypes. Among the genes encoding junctional SR proteins, RyR1 and JP1 are known as lethal genes at perinatal stages [5,9]. However, knockout mice of these genes both develop fatal impairment in SR Ca^{2+} release. In contrast, regular functioning SR Ca^{2+} stores were largely maintained in P7 *Mg56*-knockout muscle (Fig. 6). Moreover, I failed to detect MG56-mediated acylation of RyR1, JP1 and calsequestrin 2 in the in vitro enzyme assay using recombinant proteins (Fig. 12). Currently, the proposed catalytic activity of MG56 remains to be resolved.

Although I detected no cardiac abnormalities in *Mg56*-knockout suckling infant mice, MG56 probably has the same function in both skeletal and cardiac muscle. However, preferential swelling of the I-band SR is considered to be the initial phenotypic manifestation detected in *Mg56*-knockout muscle (Fig. 5 A-C), so it may provide important clues regarding the role of MG56. Although fundamental Ca^{2+}-handling functions are shared by the I-band and A-band SR compartments, there are a few reports suggesting certain functional differences between them.

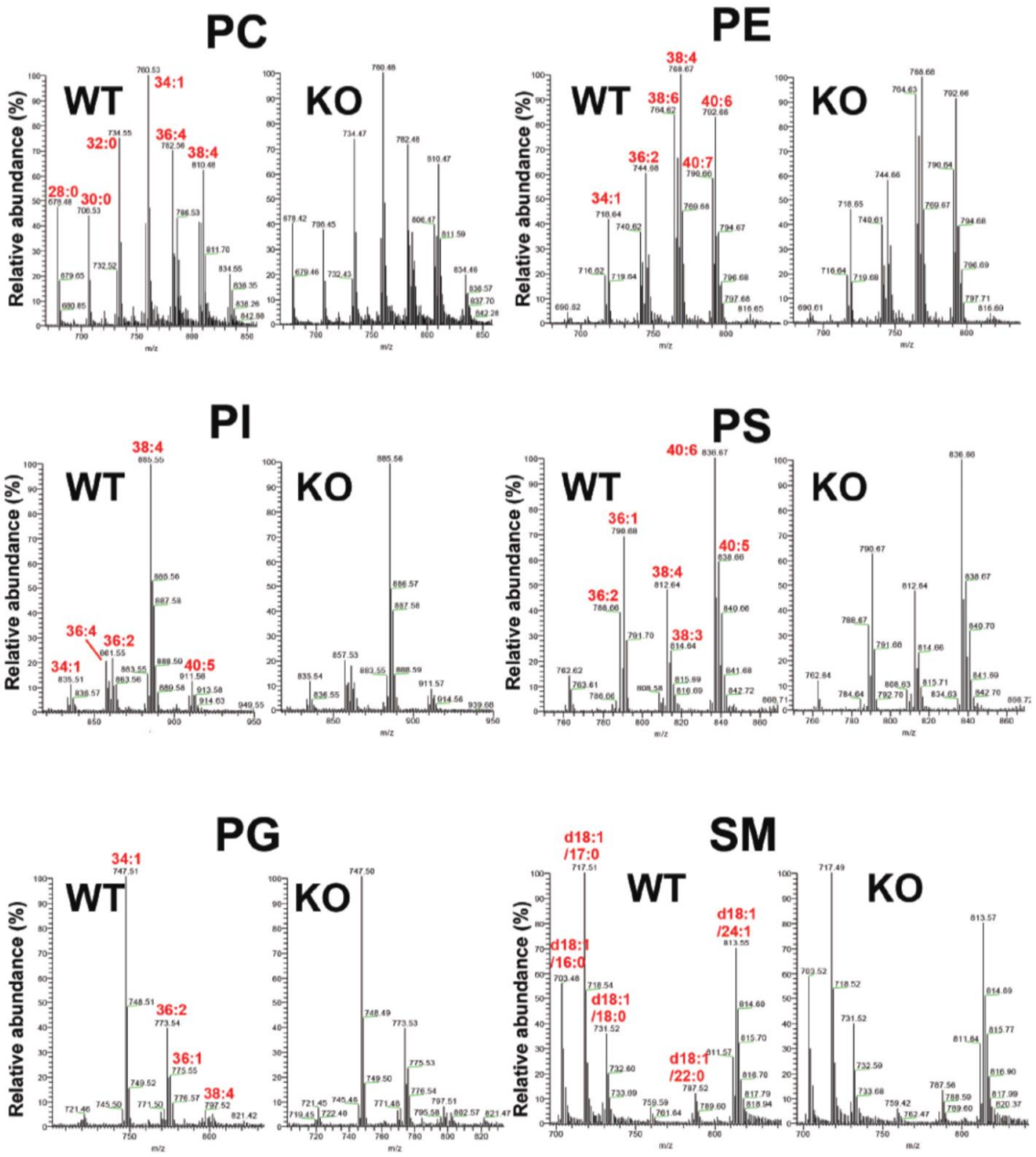

Figure 11. Quantitative analysis of phospholipids from skeletal muscle microsomes.

Total microsomes were prepared from hindlimb muscle dissected from three P9 mice, and two sets of microsomal preparations from *Mg56*-knockout and wild-type mice were subjected to LC-MS/MS analysis. Representative chart data are presented. Both total carbon and unsaturated bond numbers of the two acyl chains (red characters) are indicated for major peaks in each phospholipid class. The results suggest no essential difference in diacylphospholipid components between the knockout and wild-type muscle membranes. By means of a modified protocol, we also examined lysophospholipid species from muscle microsomes but could not find obvious alternation in the knockout muscle (data not shown).

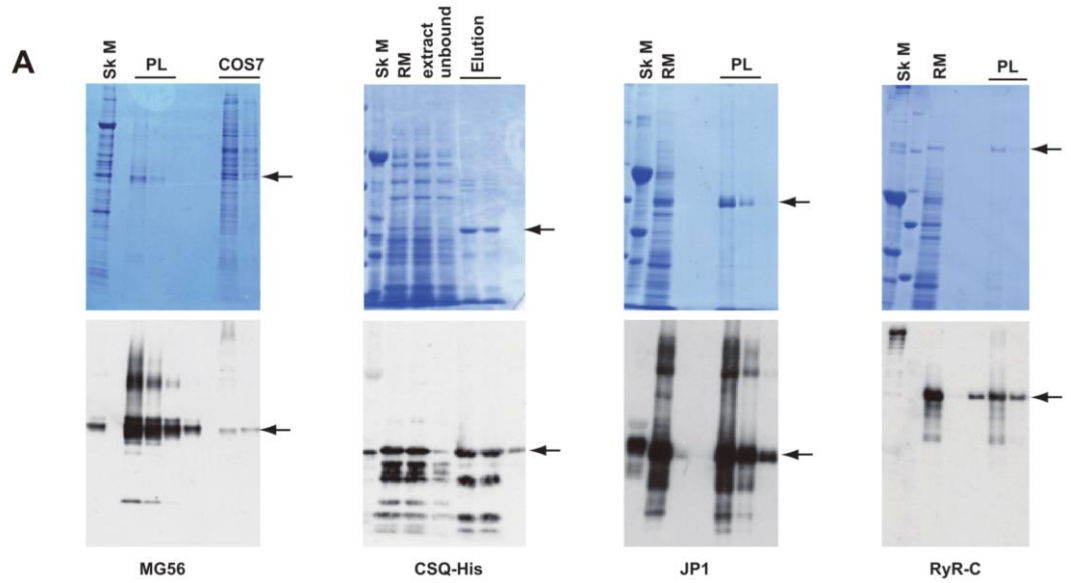

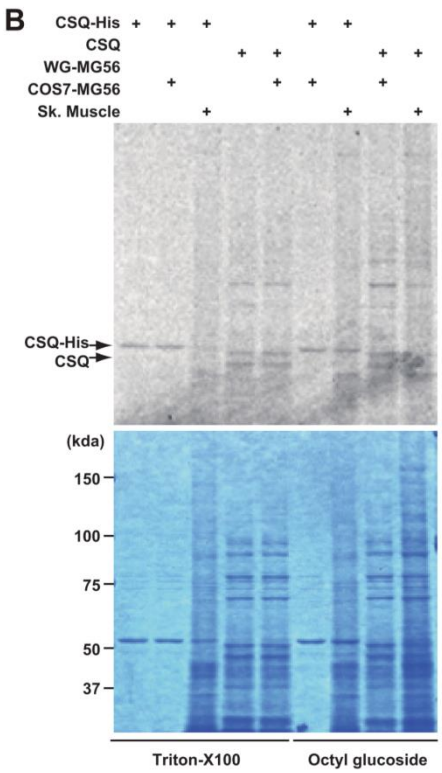

Figure 12. Palmitoylation trials using recombinant MG56.

(A) Preparation of recombinant proteins. Proteins were stained with Coomassie blue (upper panels) and immunochemically detected (lower panels). MG56 was produced in the reaction mixture of the wheat germ system (RM), and recovered in proteoliposome fractions (PL) after ultracentrifugation. MG56 was also expressed in COS7 cells and recovered in total microsomes. Calsequestrin 2 with a Hisx6 tag (CSQ-His) was produced in the reaction mixture and purified by Ni^{2+}- affinity chromatography. Furthermore, JP1 and RyR-C were also produced using the wheat germ system and recovered in proteoliposomes. Objective recombinant proteins in cDNA expression are indicated by arrows. (B) A palmitoylation trial of calsequestrin 2. The potential substrates (CSQ-His/CSQ) were reacted with recombinant MG56 from the wheat germ system (WG) or COS7 cells; skeletal muscle microsomes from adult wildtype mice (Sk M) were also examined in this trial. After incubation in the presence of ^{14}C-palmitoyl-CoA and detargent (Triton X-100 or octyl glucoside), reaction mixtures were electrophoresed and resulting gels were stained with Coomassie blue (lower panel) and subjected to fluorography (upper panel). No signal changes were observed in response to MG56, suggesting that calsequestrin is not acylated by MG56 in the muscle SR. We also conducted similar trials using JP1 and RyR-C as potential substrates but could not find any positive results.

On the basis of the sarcomere structure, the I-band SR straddles the Z-line and forms a junctional structure with the Z-disk, designated the “Z-tubule” [31]. The I-band SR likely contains abundant inositol trisphosphate receptors and seems to preferentially attach to mitochondria [32,33]. Moreover, the Sec23-positive and Ca^{2+}-dependent ER exit site to the Golgi complex is most likely associated with the I-band SR, while the rough ER lacking the export function seems to merge with the A-band SR [34]. Perhaps these compartment-specific functions are gradually established during postnatal maturation, but such processes might be disrupted in *Mg56*-knockout muscle. For example, it is plausible that a certain acyl-protein produced through MG56-mediated reaction would support proposed SR-Golgi trafficking in mature muscle. Alternatively, by committing to lipid metabolism, MG56 might improve a membrane environment favorable to the functioning of inositol trisphosphate receptors and to efficient assembling of the Ca^{2+}-dependent exit sites to the Golgi. In either of these cases, *Mg56* deficiency would inhibit protein trafficking residing in the I-band SR leading to ER stress-induced UPR activation. The present study predicts that MG56 contributes to an as-yet-unknown physiological mechanism, and future studies are required to define the molecular function of MG56 by comprehensively analyzing the knockout mice.

Materials and Methods

Biochemical and immunochemical analyses

All animal experiments were conducted with the approval of the Animal Research Committee at Kyoto University according to the regulations for animal experimentation. In the course of screening new proteins in rabbit muscle microsomes [4-8], MG56 was identified as a transmembrane protein localized in the SR. Rabbit MG56 was enriched in the heavy SR fraction from skeletal muscle, and further purified with SDS-PAGE as described previously [4]. Purified MG56 transferred onto nylon membranes (ProBlot, Applied Biosystems) was analyzed using an automated Edman sequencer (PPSQ-31, Shimadzu, Japan). A cDNA fragment was amplified with PCR primers designed based on the mouse *Hhatl* sequence data (Accession number, NM_029095). It was used as a hybridization probe for Northern blotting in adult C57BL mouse tissues and for library screening to clone the full-length mouse *Mg56* /*Hhatl* cDNA.

Immunochemical analyses were performed essentially as described previously [4], except that ×2 sampling buffer for SDS-PAGE contained 2% SDS, 8 M urea, 10% 2-mercaptoethanol, 0.01% bromphenol blue, and 40 mM Tris-HCl (pH 6.8) in this study. To prepare monoclonal antibody against mouse MG56, a synthetic peptide containing the C-terminal 21 residues was conjugated with keyhole limpet hemocyanin and injected with adjuvant into the foot pads of Wister rats. Popliteal lymph node cells were prepared from the rats and fused with NS-1 cells to yield hybridoma clones producing antibody specific to MG56. Hybridoma supernatant was used for

immunochemical analysis. Several commercial and in-house antibodies were also used in this study; anti-RyR (Thermo Scientific, MA3-925), DHPR (Sigma-Aldrich, D218), MG53[7], JPs [4], SERCA (Thermo Scientific, MA3-911), triadin (Thermo Scientific, MA3-927), TRIC channels [8], Bip/GRP78 (BD Transduction Laboratories, 610979), GRP94 (Medical & Biological Laboratories, M181-3), eukaryotic initiation factor 2 (Cell Signaling, 9721 and Santa Cruz, sc-11386), calumin [6], calsequestrin (Thermo Scientific, PA1-913) and glyceraldehyde-3-phosphate dehydrogenase (GAPDH) (Sigma-Aldrich, G9545).

Generation of knockout mice

The generation of *Mg56*-knockout mice was carried out as described previously [9]. For the construction of the targeting vector (Fig. 3A), *Hhatl* genomic DNA fragments were amplified from C57BL/6 mouse genomic DNA and used for the preparation of the short and long-arm regions. The linearized vector was transfected into embryonic stem RENKA cells derived from C57BL/6 mice [10] and several clones carrying the expected homologous mutation were selected by PCR and Southern blot analysis. Chimeric mice generated with the positive clone were crossed with C57BL/6 mice and transmitted the mutant gene to their pups. To determine the mouse genotypes, PCR analysis was conducted using Hhatl-1 (GAGTGGACCAGTCTCCTCAGAG) and Hhatl-2 (CTGTCACCGAGGCAGCTGGCAC) primers.

Histological and ultrastructural analyses were carried out as described previously [11]. Briefly, mouse tissues were fixed in 3% paraformaldehyde, 2.5% glutaraldehyde and 0.1 M sodium cacodylate (pH 7.4). After the tissues were dehydrated and embedded in Epon, ultrathin sections (~80-nm

thickness) were prepared and stained with toluidine blue for histological observation or uranyl acetate and lead citrate for ultrastructural analysis (JEM-200CX, JEOL). Mouse tissues were also fixed with phosphate buffered saline containing 3% paraformaldehyde and embedded in Tissue-Tek OCT compound (Sakura Finetek, Japan) for histological section preparations.

Muscle contraction measurements

Extensor digitorum longus (EDL) muscle bundles were dissected from mouse hindlimbs and subjected to isometric tension measurements as described previously [12]. The muscle preparation was mounted on a force transducer in a chamber containing modified Krebs-Ringer solution (121.9 mM NaCl, 4.7 mM KCl, 2.5 mM $CaCl_2$, 1.2 mM $MgCl_2$, 1.2 mM NaH_2PO_4, 15.5 mM $NaHCO_3$, and 11.5 mM glucose) constantly bubbled with 95% O_2 and 5% CO_2 at 24 °C. To induce contraction, field stimulation (10 ms duration) with supramaximal voltage was given at various frequencies for 10 s, and the developed force was recorded online using LabChart 7 software (AD Instruments). After each experiment, the muscle bundle was fixed with a 4% paraformaldehyde-containing saline for microscopic observation; cross sectional area was determined by confocal microscopy using the accompanying imaging software (FV-1000, Olympus).

Cardiac function measurements

The echocardiogram was performed using a 30-MHz microprobe (Vevo 2100, Visual Sonics) as described previously [13]. M-mode images of the interventricular septum were recorded to measure left ventricular chamber dimensions. The electrocardiogram was performed using a radiofrequency transmitter device (ETA-F20, Data Science International) as essentially described previously [14]. Transmitter leads were attached to mouse body

surfaces at clavicular and pelvic regions, and signals were recorded at 4 kHz and analyzed using the LabChart 7 software.

Gene expression analysis

Total RNA samples were prepared from mouse tissues using a commercial kit (Isogen, Nippon Gene, Japan). The RNA preparations from tibialis anterior (TA) muscle and hearts were subjected to in vitro transcription and analyzed using the GeneChip Mouse Genome 430 2.0 (Affymetrix) according to the manufacturer's instructions; the data obtained have been deposited in the NCBI-GEO database under accession number GSE64868. To analyze the detailed expression of ER stress-related genes, mRNA contents were examined by quantitative RT-PCR as described previously [14]. To analyze the tissue contents of ER stress-related proteins, mouse TA muscle was homogenized with a Physcotron (Microtec, Japan) in a buffer (150 mM NaCl, 1% NP-40, 0.5% Na deoxycholate, 0.1% SDS, 50 mM Tris-HCl, pH 8.0) containing phosphatase inhibitors (10 mM Na pyrophosphate, 100 mM NaF, 17.5 mM β-glycerophosphate, 1 mM Na orthovanadate and 1 mM EDTA) and a proteinase inhibitor cocktail. The homogenate was centrifuged at 8000×*g* for 10 min, and the resulting supernatant was analyzed by Western blotting.

Membrane lipid analysis

Membrane phospholipids were analyzed by the liquid chromatography-tandem mass spectrometry (LC-MS/MS) system consisted with a NANOSPACE SI-2 HPLC (Shiseido, Japan) and a TSQ Quantum Ultra (Thermo Fisher Scientific) triple quadropole mass spectrometer equipped with a heated electrospray ionization source as described previously [15]. To examine lysophospholipids, lipids were extracted from total muscle microsomes by methanol containing internal standards, LPA (17:0) and LPC

(17:0). The extracts were separated by a C18 Capcell Pak ACR column (Shiseido Ltd.) and subjected to the electrospray ionization MS/MS spectra acquired in the positive ion mode for LPC or the negative ion mode for other lysophospholipids. To exert diacylphospholipids analysis, lipids were extracted by 1-butanol containing internal standards (12:0/12:0 PG, 12:0/12:0 PE, 12:0/12:0 PS, 14:0/14:0 PC). The extracts were separated by a SILICA SG80 column (Shiseido) and subjected to the MS/MS spectra. The ratio between the analyte and internal standard peak areas was used for phospholipid quantification.

In vitro acylation assay

To survey MG56-mediated catalytic activity, I designed an acylation assay by reference to the reported HHAT enzyme reaction [16]. Recombinant MG56, calsequestrin 2, JP1 and RyR-C (C-terminal transmembrane portion of RyR1) [17] were prepared using a commercial wheatgerm expression system (Cell Free Sciences, Japan) according to the manufacture's instructions. Recombinant MG56 was also expressed in cultured COS7 cells and recovered in microsomal preparations. The candidate substrate proteins were reacted with MG56 in assay mixtures (20 μl) containing 0.05% detergent (Triton-X100 or octyl glucoside), 180 μM ^{14}C-palmitoyl-CoA (American Radiolabeled Chemicals), 0.5 mM dithiothreitol and 50 mM MES (pH6.5). After incubation at 30 °C for 1 h, the proteins in the assay mixtures were separated on SDS-PAGE. The gels were stained with Coomassie blue and dried for fluorography using a bioimaging analyzer (BAS 5000, Fuji, Japan) to evaluate protein palmitoylation.

PUBLICATION LIST

Bo Van, Miyuki Nishi, Shinji Komazaki, Atsuhiko Ichimura, Sho Kakizawa, Keita Nakanaga, Junken Aoki, Ki-Ho Park, Jianjie Ma, Tomomi Ueyama, Takehiro Ogata, Naoki Maruyama, Hiroshi Takeshima
Mitsugumin 56 (hedgehog acyltransferase-like) is a sarcoplasmic reticulum-resident protein essential for postnatal muscle maturation.
FEBS Lett. 2015 Apr;589(10):1095-104.

REFERENCES

[1] Ebashi, S. (1991) Excitation-contraction coupling and the mechanism of muscle contraction. Annu. Rev. Physiol. 53, 1-16.
[2] Franzini-Armstrong, C. and Protasi, F. (1997) Ryanodine receptors of striated muscles: a complex channel capable of multiple interactions. Physiol. Rev. 77, 699-729.
[3] Flucher, B.E. (1992) Structural analysis of muscle development: transverse tubules, sarcoplasmic reticulum, and the triad. Dev. Biol. 154, 245-260.
[4] Takeshima, H., Komazaki, S., Nishi, M., Iino, M. and Kangawa, K. (2000) Junctophilins: a novel family of junctional membrane complex proteins. Mol. Cell 6, 11-22.
[5] Ito, K., Komazaki, S., Sasamoto, K., Yoshida, M., Nishi, M., Kitamura, K. and Takeshima, H. (2001) Deficiency of triad junction and contraction in mutant skeletal muscle lacking junctophilin type 1. J. Cell Biol. 154, 1059-1067.
[6] Zhang, M., Yamazaki, T., Yazawa, M., Treves, S., Nishi, M., Murai, M., Shibata, E., Zorzato, F. and Takeshima, H. (2007) Calumin, a novel Ca^{2+}-binding transmembrane protein on the endoplasmic reticulum. Cell Calcium 42, 83-90.
[7] Cai, C., Masumiya, H., Weisleder, N., Matsuda, N., Nishi, M., Hwang, M., Ko, J.K., Lin, P., Thornton, A., Zhao, X., Pan, Z., Komazaki, S., Brotto, M., Takeshima, H. and Ma, J. (2009) MG53 nucleates assembly of cell membrane repair machinery. Nat. Cell Biol. 11, 56-64.
[8] Yazawa, M., Ferrante, C., Feng, J., Mio, K., Ogura, T., Zhang, M., Lin, P.H., Pan, Z., Komazaki, S., Kato, K., Nishi, M., Zhao, X., Weisleder, N., Sato, C., Ma, J. and Takeshima, H. (2007) TRIC channels are essential for Ca^{2+} handling in intracellular stores. Nature 448, 78-82.
[9] Takeshima, H., Iino, M., Takekura, H., Nishi, M., Kuno, J., Minowa, O., Takano, H. and Noda, T. (1994) Excitation-contraction uncoupling and muscular degeneration in mice lacking functional skeletal muscle ryanodine-receptor gene. Nature 369, 556-559.
[10] Mishina, M. and Sakimura, K. (2007) Conditional gene targeting on the pure C57BL/6 genetic background. Neurosci. Res. 58, 105-112.
[11] Takeshima, H., Komazaki, S., Hirose, K., Nishi, M., Noda, T. and Iino, M. (1998) Embryonic lethality and abnormal cardiac myocytes in mice lacking ryanodine receptor type 2. EMBO J. 17, 3309-3316.
[12] Yoshida, M., Minamisawa, S., Shimura, M., Komazaki, S., Kume, H., Zhang, M., Matsumura, K., Nishi, M., Saito, M., Saeki, Y., Ishikawa, Y., Yanagisawa, T. and Takeshima, H. (2005) Impaired Ca^{2+} store functions in skeletal and cardiac muscle cells from sarcalumenin-deficient mice. J. Biol. Chem. 280, 3500-3506.
[13] Ogata, T., Naito, D., Nakanishi, N., Hayashi, Y.K., Taniguchi, T., Miyagawa, K., Hamaoka, T., Maruyama, N., Matoba, S., Ikeda, K., Yamada, H., Oh, H. and Ueyama, T. (2014) MURC/Cavin-4 facilitates recruitment of ERK to caveolae and concentric cardiac hypertrophy induced by a1-adrenergic receptors. Proc. Natl. Acad. Sci. USA 111, 3811-3816.
[14] Yamazaki, D., Tabara, Y., Kita, S., Hanada, H., Komazaki, S., Naitou, D., Mishima, A., Nishi, M., Yamamura, H., Yamamoto, S., Kakizawa, S., Miyachi, H., Yamamoto, S., Miyata, T., Kawano, Y., Kamide, K., Ogihara, T., Hata, A., Umemura, S., Soma, M., Takahashi, N., Imaizumi, Y., Miki, T., Iwamoto, T. and Takeshima, H. (2011) TRIC-A channels in vascular smooth muscle contribute to blood pressure maintenance. Cell Metab.

14, 231-241.
[15] Inoue, A., Arima, N., Ishiguro, J., Prestwich, G.D., Arai, H. and Aoki, J. (2011) LPA-producing enzyme PA-PLA1 a regulates hair follicle development by modulating EGFR signalling. EMBO J. 30, 4248-4260.
[16] Buglino, J.A. and Resh, M.D. (2010) Identification of conserved regions and residues within hedgehog acyltransferase critical for palmitoylation of sonic hedgehog. PLoS One 5, e11195.
[17] Bhat, M.B., Zhao, J., Takeshima, H. and Ma, J. (1997) Functional calcium release channel formed by the carboxyl-terminal portion of ryanodine receptor. Biophys. J. 73, 1329-1336.
[18] Hofmann, K. (2000) A superfamily of membrane-bound O-acyltransferase with implications for wnt signaling. Trends Biochem. Sci. 25, 111-112.
[19] Yang, J., Brown, M.S., Liang, G., Grishin, N.V. and Goldstein, J.L. (2008) Identification of the acyltransferase that octanoylates ghrelin, an appetite-stimulating peptide hormone. Cell 132, 387-396.
[20] Dodge, M.E., Moon, J., Tuladhar, R., Lu, J., Jacob, L.S., Zhang, L.S., Shi, H., Wang, X., Moro, E., Mongera, A., Argenton, F., Karner, C.M., Carroll, T.J., Chen, C., Amatruda, J.F. and Lum, L. (2012) Diverse chemical scaffolds support direct inhibition of the membrane-bound O-acyltransferase porcupine. J. Biol. Chem. 287, 23246-23254.
[21] Abe, Y., Kita, Y. and Niikura, T. (2008) Mammalian Gup1, a homolog of Saccharomyces cerevisiae glycerol uptake/transporter 1, act as a negative regulator for N-terminal palmitoylation of sonic hedgehog. FEBS J. 275, 318-331.
[22] Saito, A., Seiler, S., Chu, A. and Fleischer, S. (1984) Preparation and morphology of sarcoplasmic reticulum terminal cisternae from rabbit skeletal muscle. J. Cell Biol. 99, 875-885.
[23] Luff, A.R. and Atwood, H.L. (1971) Changes in the sarcoplasmic reticulum and transverse tubular system of fast and slow skeletal muscles of the mouse during postnatal development. J. Cell Biol. 51, 369-383.
[24] Boncompagni, S., Protasi, F. and Franzini-Armstrong, C. (2012) Sequential stages in the age-dependent gradual formation and accumulation of tubular aggregates in fast twitch muscle fibers: SERCA and calsequestrin involvement. Age (Dordr) 34, 27-41.
[25] Walter, P. and Ron, D. (2011) The unfolded protein response: from stress pathway to homeostatic regulation. Science 334, 1081-1086.
[26] Hetz, C. (2012) The unfolded protein response: controlling cell fate decisions under ER stress and beyond. Nat. Rev. Mol. Cell Biol. 13, 89-102.
[27] Vannuvel, K., Renard, P., Raes, M. and Arnould, T. (2013) Functional and morphological impact of ER stress on mitochondria. J. Cell. Physiol. 228, 1802-1818.
[28] Yoshida, H., Matsui, T., Yamamoto, A., Okada, T. and Mori, K. (2001) XBP1 mRNA is induced by ATF6 and spliced by IRE1 in response to ER stress to produce a highly active transcription factor. Cell 107, 881-891.
[29] Flamment, M., Hajduch, E., Ferré, P. and Foufelle, F. (2012) New insights into ER stress-induced insulin resistance. Trends Endocrinol. Metab. 23, 381-390.
[30] Volmer, R., van der Ploeg, K. and Ron, D. (2013) Membrane lipid saturation activates endoplasmic reticulum unfolded protein response transducers through their transmembrane domains. Proc. Natl. Acad. Sci. USA 110, 4628-4633.
[31] Ogata, T. and Yamasaki, Y. (1990) High-resolution scanning electron microscopic studies on the three-dimensional structure of the transverseaxial tubular system,

sarcoplasmic reticulum and intercalated disc of the rat myocardium. Anat. Rec. 228, 277-287.
[32] Powell, J.A., Carrasco, M.A., Adams, D.S., Drouet, B., Rios, J., Müller, M., Estrada, M. and Jaimovich, E. (2001) IP_3 receptor function and localization in myocytes: an unexplored Ca^{2+} signaling pathway in skeletal muscle. J. Cell Sci. 114, 3673-3683.
[33] Ogata, T. and Yamasaki, Y. (1997) Ultra-high-resolution scanning electron microscopy of mitochondria and sarcoplasmic reticulum arrangement in human red, white, and intermediate muscle fibers. Anat. Rec. 248, 214-223.
[34] Kaisto, T. and Metsikkö, K. (2003) Distribution of the endoplasmic reticulum and its relationship with the sarcoplasmic reticulum in skeletal myofibers. Exp. Cell Res. 289, 47-57.
[35] Rios-Esteves, J., Haugen, B. and Resh, M.D. (2014) Identification of key residues and regions important for porcupine-mediated Wnt acylation. J. Biol. Chem. 289, 17009-17019.

ACKNOWLEDGEMENTS

Great gratitude is expressed to Professor Hiroshi Takeshima, Graduate School of Pharmaceutical Science, Kyoto University for his constant guidance and intense encouragement through the course of this work. Appreciation is also given to Associate Professor Miyuki Nishi and Associate Professor Sho Kakizawa, especially to Assistant Professor Atsuhiko Ichimura for his help at the end of the doctoral course. The author is also deeply grateful to the former and present members of Department of Biological Chemistry, Graduate School of Pharmaceutical Science, Kyoto University. And the same gratitude is given to Dr. Shinji Komazaki and Ms. Reiko Inomata for histological analysis (Saitama Medical University), Dr. Junken Aoki (Tohoku University) for quantitative analysis of phospholipids, Drs. Natsuo Ueda (Kagawa University) and Nozomu Kono (University of Tokyo) for phospholipid enzyme assay, Drs. Ki-Ho Park (The Ohio State University), Kazutoshi Mori (Kyoto University) and Masahiko Hoshijima (University of California, San Diego) for insightful suggestions. Lastly, I would like to thank my parents and members of my family for mental encouragement and economics support.